scientific reports

Check for updates

OPEN

Estimation of outer-wall length in optimizing cochlear implantation in malformed inner ears

Afrah Alshalan[1]✉, Yassin Abdelsamad[2], Asma Alahmadi[3], Francesco Santoro[4], Salman Alhabib[5], Fida Almuhawas[5], Farid Alzhrani[5], Abdulrahman Alsanosi[5] & Anandhan Dhanasingh[6]

Estimation of cochlear length is gaining attention in the field of cochlear implants (CIs), mainly for selecting of CI electrode lengths. The currently available tools to estimate the cochlear duct length (CDL) are only valid for normal inner anatomy. However, inner ear malformation (IEM) types are associated with different degrees of cystic apices, limiting the application of CDL equations of normal anatomy inner ear. Therefore, this study aimed to understand the degree to which the outer wall (OW) is observed in different malformation types and to formulate mathematical equations to estimate the OW length (OWL) from cochlear parameters, namely the basal turn diameter (A-value) and width (B-value). Three-dimensional (3D) segmentation of promontory and fluid parts of the inner ear was performed to understand the extent to which the OW is visible to measure the OWL manually. Enlarged vestibular aqueduct syndrome (EVAS) was diagnosed in 37 ears, which consistently showed the extent of the OW to an angular depth of 540°, beyond which the cystic apex starts. Incomplete partition (IP) type I was observed in 30 ears, with the OW extending to only 360° of angular depth. IP type II was observed in 35 ears, with the OW extending to 450° of angular depth. IP type III was identified in 24 ears, with the OW observed for 540° of angular depth. Cavity-type malformations were observed in 36 ears, and circumference was measured in the axial view. A strong positive linear correlation was observed between the manually measured OWL and cochlear parameters for all malformation types analyzed. A multiple linear regression model was applied to formulate mathematical equations, which was further used to create a software application for estimating OWLs in IEM types, using cochlear parameters as inputs.

Keywords Cochlear implant, Inner ear malformation, Outer wall length, Electrode array, Cochlear parameters

Cochlear implant (CI) is a widely accepted treatment option for patients with severe-to-profound sensorineural hearing loss[1,2]. According to the World Health Organization, an estimated 430 million individuals may benefit from CIs[3]. Hearing outcomes with CIs are highly variable and are affected by several factors, including the duration of deafness, age at implantation, preoperative hearing level, amount of audio processor usage per day, the remaining number of neuronal elements in the cochlea, and etiology of hearing loss[4–7]. While all these factors are difficult to control, the effective placement of electrode matching cochlear size is feasible by proper planning from the pre-operative radiographs[8]. A recent systematic literature review on electrode insertion depth reported a positive effect on the hearing outcome with CI[9].

Estimation of cochlear duct length (CDL) to match electrode length in normal anatomy inner ear is an established research topic in the CI field[10,11]. These mathematical equations to estimate CDL were validated for the normal inner ear anatomy[12]. However, to our limited knowledge, only a single report exists on the estimation of effective cochlear lengths in the malformed inner ears[13].

Among congenitally deaf-born children, approximately 15–20% of the population is reported to have some degree of malformed inner ear anatomy[14]. Anomalies such as cavity-type malformation, incomplete partition

[1]Department of Otolaryngology-Head and Neck Surgery, College of Medicine, Jouf University, PO Box 72418 , Skaka, Aljouf 23235, Saudi Arabia. [2]Research Department, MED-EL, Riyadh, Saudi Arabia. [3]Maternity and Children Hospital, Makkah, Saudi Arabia. [4]Universita Campus Bio-Medico di Roma, Rome, Italy. [5]King Abdullah Ear Specialist Center (KAESC), College of Medicine, King Saud University, Riyadh, Saudi Arabia. [6]Research and Development, MED-EL, Innsbruck, Austria. ✉email: amalshalan@ju.edu.sa

(IP) type I, cochlear hypoplasia (CH), IP type II, and enlarged vestibular aqueduct syndrome (EVAS) are the result of developmental arrest at different stages of human embryology[15,16].

The present study aims to propose a methodology for estimating a safe and effective electrode insertion depth in different types of inner ear malformation (IEM). The size and shape of the cavity-type malformation vary among populations, and a single measurement of the cavity in the axial plane can predict the cavity circumference; therefore, an electrode of suitable length can be recommended as per our earlier study[17]. IP type I is characterized by a completely cystic cochlear portion with the outer wall (OW) of the cochlea observed for 360° of angular turns. A single measurement in the oblique coronal plane measuring the diameter of the cochlear portion showing the cochlear entrance can predict the OW length (OWL) for 360°, which can then be used to choose the effective electrode length in IP type I, as per our earlier study. IP type II is characterized by a part of the basal turn separated from the cystic middle and apical turn with the OW observed for 450° of angular turns. The EVAS has more of the basal turn developed, leaving the apical portion of the cochlea cystic, with the OW observed for 540° of angular turns[18]. In IP type III, if the electrode optimally goes inside the cochlear portion, avoiding entering the internal auditory canal (IAC), it covers close to 540° of angular depth as per our clinical experience.

To the best of our knowledge, there are no reported solutions available for measuring or estimating the OWLs for a safe and effective insertion depth in these malformation types to choose an appropriate electrode length. This motivated us to investigate EVAS, IP type I, IP II, IP III, and cavity-type malformations in detail to propose a solution for estimating OWL and to consolidate our previous work to formulate mathematical equations to estimate OWL in IEM types with basic cochlear parameters as inputs.

Materials and methods

Image database

This retrospective study examined 162 ears with different types of IEMs. These ears underwent high-resolution preoperative computed tomography (CT) and received CIs at our tertiary hearing implant centers within the Middle East region. Ears with poor CT resolution or normal inner ear anatomy were excluded from the study. Based on the radiologists' reports, only scans with IEM, including EVAS, IP type I, IP II, IP III, and cavity type, were selected for this study. We deliberately excluded the CH-type malformation from this study because of the high variation in the overall morphology of the inner ear, limiting us from formulating a mathematical equation to estimate the OWL for cochlear hypoplasia type malformation.

Image analyses

Three-dimensional (3D) segmentation of the inner ear fluid as a solid model was performed using 3D Slicer software (https://www.slicer.org), following the steps described elsewhere[19] (Fig. 1A). Using the solid model, the mid-modiolar section of the inner ear was captured to accurately identify the inner ear anatomical type, following the pattern of the outer contour, as described elsewhere (Fig. 1B). A shell model of the inner ear was created by 3D segmentation of the promontory bone around the inner ear to visualize the extent to which the

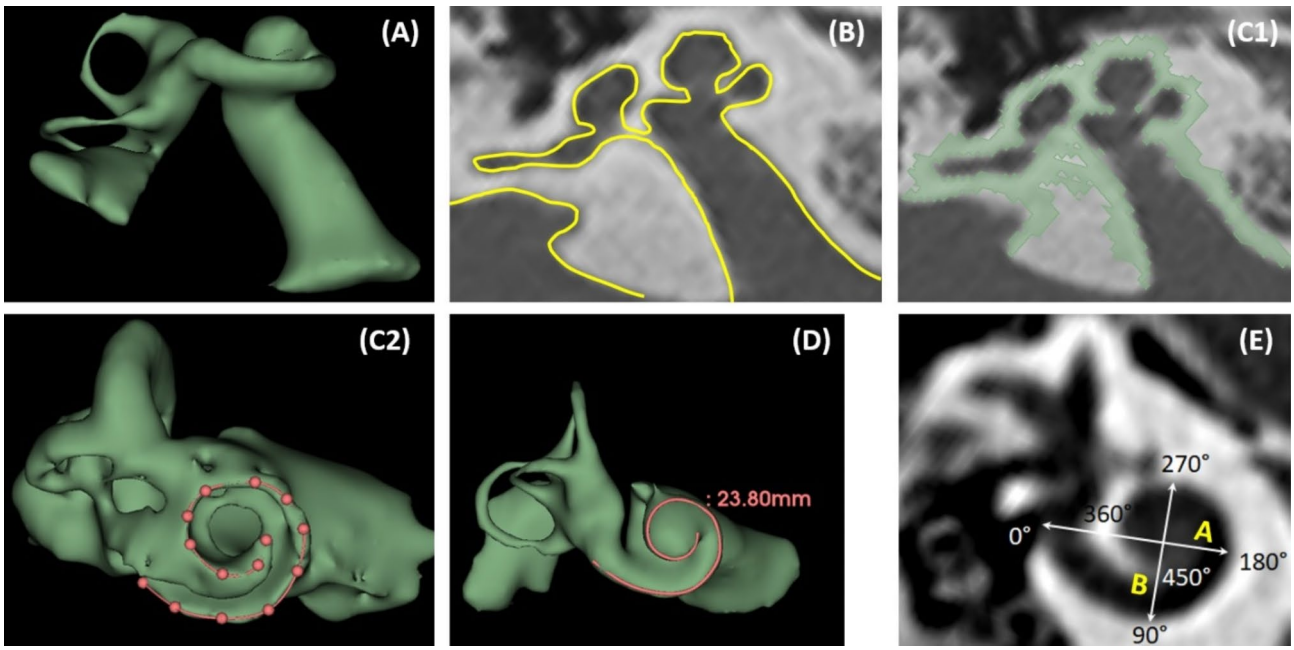

Fig. 1. Three-dimensional (3D) segmented solid model of the inner ear in axial view (**A**). The outer contour of the mid-modiolar section (**B**). Promontory bone was captured to create the shell model (**C1**). Shell model of the inner ear showing the extent of the outer wall (**C2**). Manual measurement of outer wall length (**D**). Measurement of diameter and width of the basal turn (**E**).

OW was visible before the cystic portion began (Fig. 1C1, axial view; Fig. 1C2, coronal view). From the solid model, OWL was manually measured in agreement between the two CI consultants for each of the samples taken for analysis (Fig. 1D). Using 3D images as a reference and adjusting the coronal image to capture the basal turn of the cochlea in cochlear view, the cochlear diameter (A-value) and width (B-value) were measured (Fig. 1E). The A-value represents the largest linear distance from the center of round window to the furthest point on the opposite lateral wall, passing through the modiolus. The B-value represents the width of the basal turn drawn perpendicular to the A-value[13].

Statistical analysis

All statistical analyses were performed using Microsoft Excel (https://www.microsoft.com/en-us/microsoft-365/excel). The A- and B-values were individually plotted against OWL to observe the correlation between the two parameters using regression analysis. Multiple linear regression analysis was performed to formulate mathematical equations to estimate OWL from the A- and B-values for each anatomical type. The relative error (%) between the measured and estimated OWL was calculated by dividing the difference between the measured (M) and estimated (E) OWL values by the measured OWL value[13].

$$\text{The relative error}\,(\%) = ([\mathrm{M} - \mathrm{E}]\,/\mathrm{M}) * 100$$

A two-sample *t*-test, assuming unequal variance, was performed to check for statistical significance among the variables.

Software application to estimate OWL

Visual Studio 2010 for Windows Desktop (https://visualstudio.microsoft.com/) was used in the architecture of the software application/calculator to estimate OWL from the cochlear parameters for each anatomical type. The calculator runs mathematical equations to estimate the OWL using the A- and B-values as inputs. The user must follow the following three steps. In step 1, the user should 3D segment the inner ear to visualize the mid-modiolar section and the cochlear view to recognize the pattern to identify the anatomical type. In step 2, the cochlear view is used to measure the A- and B-values. In step 3, the A- and B-values are used as inputs to estimate the OWL in the software application.

Ethics declarations

The study was rigorously carried out in complete accordance with the ethical guidelines delineated in the Declaration of Helsinki. Additionally, it received formal approval from the Institutional Review Board at King Saud University, denoted by Approval Number (IRB No. 22/0084/IRB).

Informed consent

Informed consent was officially waived by the same authoritative local committee (Institutional Review Board at King Saud University), a decision made in recognition of the study's retrospective nature.

Results

Image database

In total, 162 ears of different IEM types were identified from the image database. Table 1 summarizes the malformation types and number of cases identified for each type. EVAS; IP types I, II, and III; and the common cavity were the different anatomical types identified. The number of IP III cases was lower than that of other anatomical types.

Image analyses

A 3D segmented shell model of five different inner ear anatomical types revealed that the OW was consistently observed for an angular insertion depth (AID) of 540° in EVAS, 450° in IP II, and 360° in IP I as a distinct feature of these anatomical types. Beyond these AIDs, the cochlear portion appeared cystic. In the case of IP III, the OWL was measured for 540°, based on our clinical experience with inserting electrodes to that insertion depth. Figure 2 displays the measured and average A- and B-values and OWL for all the samples analyzed. The A-values of EVAS compared to those of the cochleae with IP I ($p < 0.001$) and IP III ($p < 0.001$) were significantly different but not with IP II ($p = 0.1$). The B-values of EVAS were significantly different from those of the cochleae with IP II ($p = 0.01$), IP I ($p < 0.001$), and IP III ($p < 0.001$). The OWL of EVAS measured at 540° of AID was significantly different from that of IP I measured at 360° AID ($p < 0.001$), IP II measured at 450° AID ($p < 0.001$), and IP III

Malformation type	Number of ears
EVAS	37 (22.8%)
IP I	30 (18.5%)
IP II	35 (21.6%
CC	36 (22.3%)
IP III	24 (14.8%)
Total	162 (100%)

Table 1. Number of ears identified under each malformation type.

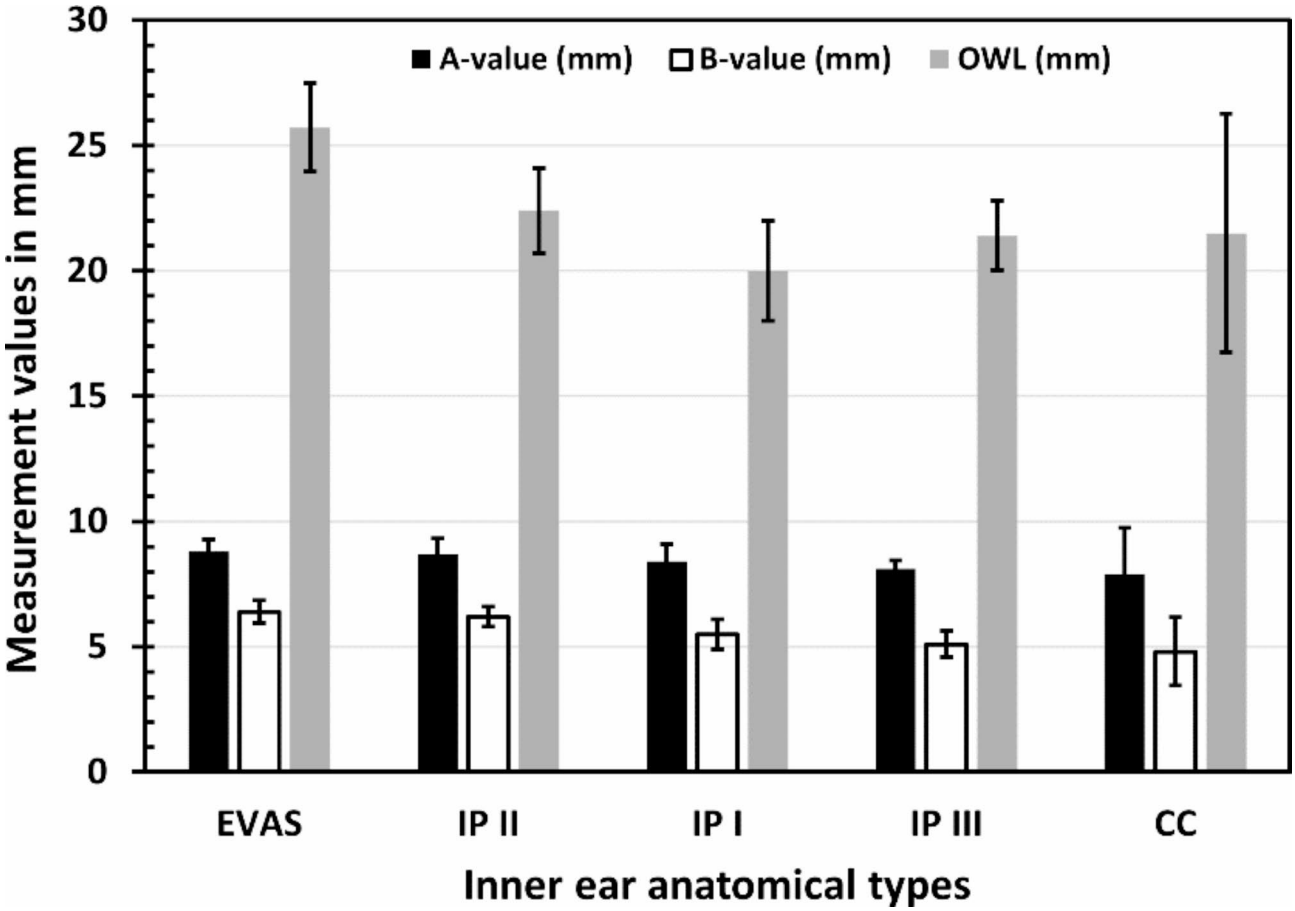

Fig. 2. An illustration of measured A-, B-values, and outer wall lengths of all anatomical types taken in this study.

measured at 540° AID ($p < 0.001$). Figure 3 shows the illustration of how OWL is measured from the shell model (column A). Regression analysis showed a positive linear correlation between both the A- and B-values and the OWL for all anatomical types taken in this study as shown in columns B and C respectively.

Estimation of OWL from basic cochlear parameters

The multiple linear regression model used to estimate OWL from the A- and B-values yielded the following mathematical equations:

$$EVAS\ for\ 540^{\circ}\ of\ AID = 0.84 \times\ A + 2.5 \times\ B + 2.11 \tag{1}$$

$$IP\ II\ for\ 450^{\circ}\ of\ AID = 1.3 \times\ A + 1.65 \times\ B + 1.0 \tag{2}$$

$$IP\ I\ for\ 360^{\circ}\ of\ AID = 0.73 \times\ A + 2 \times\ B + 3.03 \tag{3}$$

$$IP\ III\ for\ 540^{\circ}\ of\ AID = 1.2 \times\ A + 2.2 \times\ B - 2.44 \tag{4}$$

$$Circumference\ of\ CC = (2.2 \times\ long\ axis) + (0.66 \times\ short\ axis) + 0.6 \tag{5}$$

Table 2 in the supplement displays the OWL values measured manually and those estimated using Eqs. 1–5. The p-value (0.001) confirmed that the measured and estimated OWL values were not statistically different.

Software application to estimate OWL from cochlear parameters

A calculator for estimating the OWL for different inner ear anatomies is shown in Fig. 4. Selecting the A- and B-values from the drop-down box and clicking on the appropriate inner ear anatomical type in step 3 provides the estimated OWL and the matching electrode length. Please click **here** to access the OWL calculator.

Discussion

The optimal placement of electrodes inside the cochlea is believed to be the basis for successful CI treatment, even in IEM types. In most of the IEM types, some part of the apex is cystic, and pushing the electrode into the cystic apex could lead to suboptimal placement of the electrode, as reported by Hagr et al[20]. This motivated us to

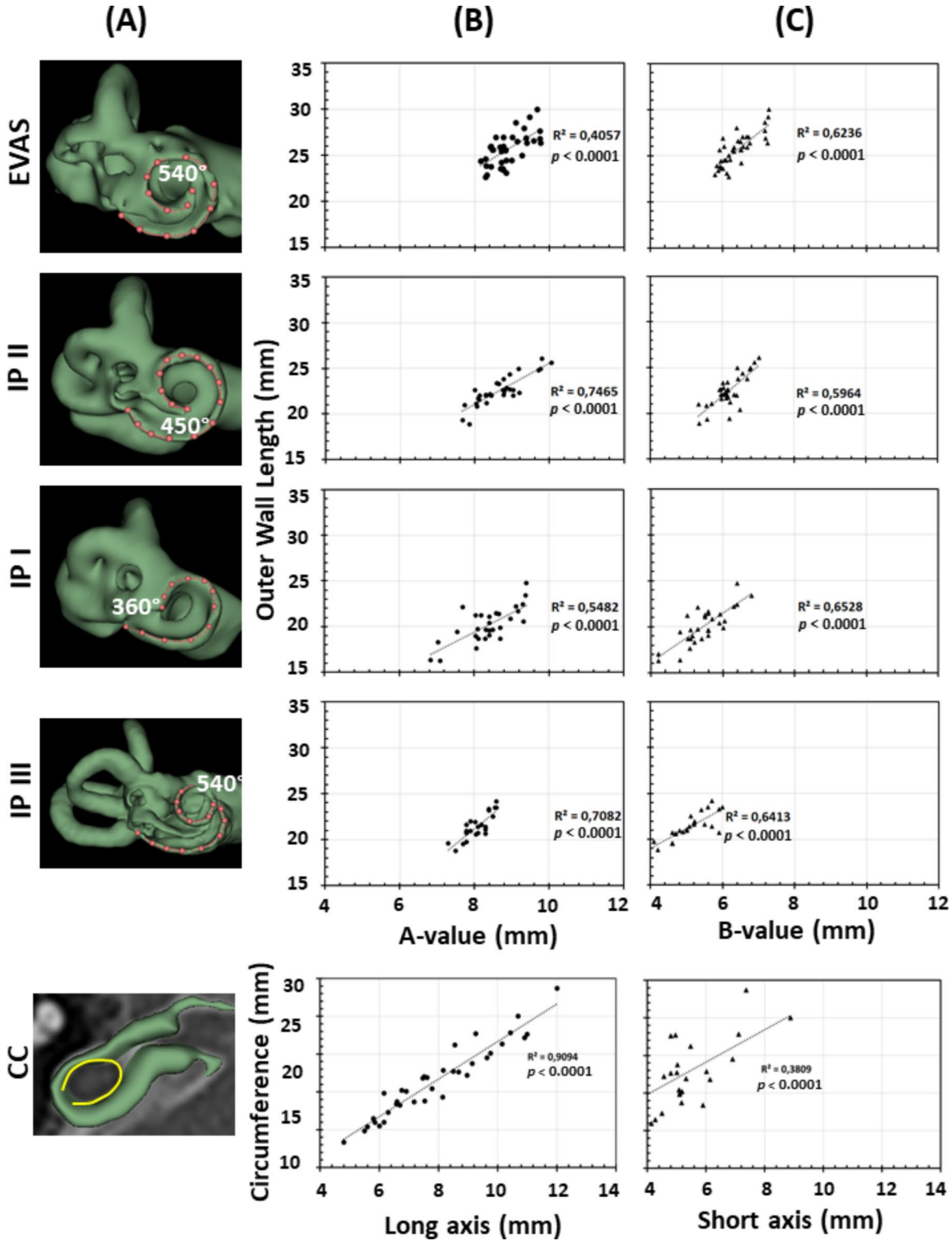

Fig. 3. Column A shows the shell model of five different malformation types. Column B shows the correlation between the A-value and OWL. Column C shows the correlation between the B-value and OWL. EVAS: enlarged vestibular aqueduct syndrome; IP I: incomplete partition type I; IP II: incomplete partition type II; IP III: incomplete partition type III; CC: common cavity; OWL: outer wall length.

investigate the anatomy of the malformed inner ear to determine how far the OW was visible before the cystic apex began.

Our previous work estimated the basal turn length (BTL, 360° of AID) in different IEM types[13]. That work was motivated by the early work of Adunka et al., who estimated the BTL to choose electrode length in patients

Types	EVAS			IP II			IP I			CC			IP III		
No	M	E	Error %	M	E	Error %	M	E	Error %	M	E	Error %	M	E	Error %
1	23.9	23.7	0.6	22.5	22.6	-0.4	21.4	20.5	4.3	27.8	28.2	-1.5	22.0	21.2	3.3
2	25.6	24.9	5.1	21.1	20.8	1.0	21.2	18.9	10.8	21.8	21.1	3.3	21.6	21.0	2.9
3	23.1	24.8	-7.6	20.1	20.6	0.8	22.4	22.6	-0.8	26.2	23.0	12.1	20.6	21.5	-4.1
4	24.4	23.8	2.3	24.3	23.5	3.7	20.1	21.9	-6.5	27.6	27.9	-1.3	23.3	23.1	0.8
5	26.4	28.5	-7.7	24.9	23.5	5.6	21.3	21.2	0.6	30.0	29.9	0.1	23.5	23.6	-0.5
6	22.9	23.6	-3.1	22.1	21.9	0.9	17.6	19.1	-8.3	24.5	26.4	-7.6	19.5	20.0	-2.4
7	23.6	24.4	-3.3	23.3	22.2	4.9	18.7	19.1	-2.4	19.3	20.0	-8.5	19.8	19.6	0.6
8	23.4	24.2	-3.4	22.7	22.5	0.9	19.7	19.5	0.8	33.7	31.8	5.4	21.4	22.6	-5.8
9	25.0	25.3	-1.3	22.1	22.0	0.5	16.3	17.6	-7.9	21.9	20.8	4.7	20.7	21.8	-5.2
10	26.5	26.1	1.7	22.8	22.5	1.5	18.3	18.6	-1.4	20.2	18.8	6.5	20.7	20.9	-0.8
11	23.8	24.0	-0.9	22.0	21.4	0.7	19.9	21.4	-9.7	20.4	21.1	-3.2	20.6	20.8	-1.5
12	24.6	24.6	0.0	21.8	21.7	0.2	19.1	20.4	-6.7	22.0	19.2	12.7	18.8	19.1	-1.6
13	25.6	25.0	2.5	26.1	25.3	2.9	18.9	19.2	-1.3	23.7	24.0	-1.2	21.0	20.7	1.2
14	25.5	25.2	1.1	25.6	25.5	0.5	18.7	19.8	-5.8	15.5	15.9	-2.7	20.8	20.6	1.1
15	26.9	25.0	7.1	22.0	22.7	-3.0	21.7	20.9	3.5	26.3	25.3	4.0	22.5	22.4	0.4
16	26.6	26.3	1.3	22.1	22.3	-0.8	19.4	18.1	6.5	25.1	24.7	1.6	21.9	21.5	1.9
17	27.0	25.7	4.7	19.4	20.2	-4.3	22.1	19.2	13.0	20.1	19.1	4.3	20.9	20.7	1.0
18	27.0	26.5	2.0	18.9	20.1	-6.4	21.0	20.9	-0.6	17.3	17.4	-0.8	19.6	19.1	2.1
19	27.0	26.1	3.2	23.4	22.3	4.6	19.7	19.3	1.8	15.4	15.3	0.2	23.2	22.5	2.9
20	25.9	25.0	3.5	23.8	23.1	3.2	22.2	22.3	-0.5	22.9	22.5	1.4	24.2	23.3	3.5
21	24.5	24.8	-1.2	21.7	21.6	0.5	23.4	23.4	-0.3	22.7	22.6	0.4	23.5	23.2	1.2
22	24.5	24.8	-1.2	21.0	19.8	5.3	24.7	22.7	8.3	18.7	18.6	0.7	21.6	22.2	-2.7
23	30.0	28.4	5.2	25.0	24.9	0.1	21.3	20.0	5.8	18.2	17.7	2.8	21.4	21.5	-0.3
24	29.2	28.3	3.2	24.8	24.8	0.0	19.6	20.4	-3.8	14.8	14.7	0.6	21.1	21.8	-3-3
25	28.0	25.9	7.4	22.0	21.9	0.8	21.1	20.2	4.4	18.7	18.9	-1.2	-	-	-
26	26.4	26.9	-1.9	22.6	21.2	6.2	19.7	20.4	-4.0	18.7	18.5	0.8	-	-	-
27	28.6	27.7	2.9	21.2	22.1	-4.2	20.4	20.9	-2.7	16.0	16.5	-3.8	-	-	-
28	26.9	28.3	-5.3	22	22.1	0.6	18.7	19.6	-5.0	19.8	17.5	11.6	-	-	-
29	27.7	28.2	-1.9	22.3	22.5	0.4	16.3	16.6	-2.1	13.3	13.6	-2.0	-	-	-
30	24.2	25.7	-6.2	22.0	22.4	-1.8	17	17.2	-1.1	18.4	18.9	-3.2	-	-	-
31	26.0	24.3	6.4	22.3	23.0	-3.1	-	-	-	15.9	16.2	-1.7	-	-	-
32	25.6	25.5	0.4	22.6	22.9	-1.3	-	-	-	16.5	16.2	1.6	-	-	-
33	25.9	26.1	-0.7	20.4	23.3	-14.3	-	-	-	27.7	24.2	12.4	-	-	-
34	26.0	25.9	0.3	19.4	22.4	-15.0	-	-	-	27.2	27.2	-0.2	-	-	-
35	25.6	25.8	-0.9	23.8	24.5	-3.1	-	-	-	22.2	23.3	-5.1	-	-	-
36	23.6	24.4	-3.5	-	-	-	-	-	-	22.6	22.8	-1.0	-	-	-
37	22.7	24.5	-7.9	-	-	-	-	-	-	-	-	-	-	-	-
Mean ± Std. dev.	**25.7 ± 1.8**	**25.6 ± 1.4**	**0.0 ± 4.0**	**22.4 ± 1.7**	**22.5 ± 1.3**	**-0.4 ± 4.6**	**20.1 ± 1.9**	**20.1 ± 1.6**	**-0.3 ± 5.5**	**21.5 ± 4.8**	**21.2 ± 4.5**	**1.1 ± 5.1**	**21.5 ± 1.4**	**21.4 ± 1.3**	**-0.2 ± 2.7**

Continued

Types	EVAS			IP II			IP I			CC			IP III		
No	M	E	Error %	M	E	Error %	M	E	Error %	M	E	Error %	M	E	Error %
Range	22.7–30	23.6–28.5	-7.9–7.4	18.9–26.1	19.8–25.5	-15.4–6.2	16.3–24.7	16.6–23.4	-8.4–13.1	13.3–33.7	13.6–31.8	-8.5–12.7	18.8–24.2	19.1–23.6	-5.8–3.5
p	0.87			0.90			0.99			0.77			0.93		

Table 2. Outer wall length (OWL) in mm as measured and estimated, along with the relative error between the two values in percentage. EVAS: enlarged vestibular aqueduct syndrome; IP I: incomplete partition type I; IP II: incomplete partition type II; IP III: incomplete partition type III; CC: common cavity; M: measured; E: estimated.

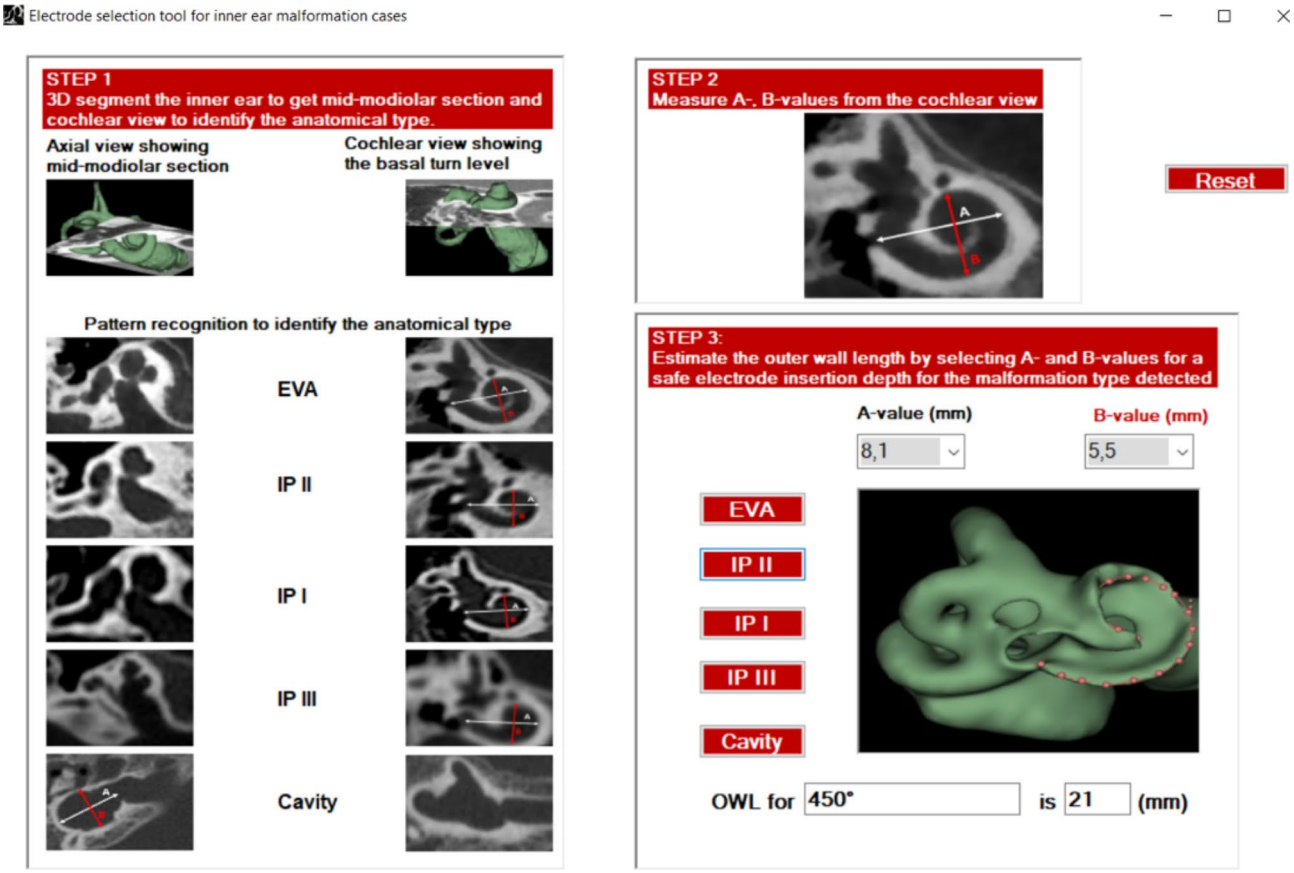

Fig. 4. Screenshot of a softwarer application showing the three steps to be followed to estimate the OWL in five different malformation types.

with functional low-frequency residual hearing[21]. In the present study, a systematic analysis of several CT scans of IEMs after creating the shell model of the inner ear showed that the OWL was observed consistently for 540° of AID in EVAS, 360° in IP I, 450° in IP II, and approximately 540° in IP III. Manual measurements of the A- and B-values and OWLs led to the formulation of mathematical equations to estimate the OWL for effective electrode insertion depths in different IEM types. An advanced DICOM (Digital Imaging & Communications in Medicine) viewer such as OTOPLAN® can orient the inner ear automatically to the cochlear view, minimizing the effort needed to measure the cochlear parameters such as A- and B-values.

The normal anatomy inner ear has spiral ganglion cell bodies distributed up to 680° of AID[22,23], whereas in IEM types, the neural architecture is not entirely known. Graham et al. reported that nerve fibers sprout from the IAC and spread along the inner surface of the OW of the common cavity[24]. This is supported by Yamazaki et al., who showed that electrode channels closer to the fundus region elicited an electrically evoked auditory brainstem response, confirming the presence of neural elements in the common cavity malformation type[25]. Histopathological evaluation of temporal bones with IEMs by Monsanto et al. revealed that IP type I, characterized by an ovoid-shaped cochlear portion, had spiral ganglion cells along the posterior-inferior wall of the cochlear portion. In IP type II, severe loss of nerve fibers and spiral ganglion cells in Rosenthal's canal was observed even though the IAC and bony cochlear nerve canal were normal[26]. All these variations in the presence of nerve fibers and neuronal cell bodies could contribute to variations in hearing outcomes with CI among malformation types.

The OWLs measured manually from EVAS ($n=37$) samples, ranging from a minimum of 22 mm to a maximum of 30 mm, shows the necessity for electrodes to be available in different lengths. The range of OWLs measured from IP II ($n=35$) samples varied between 19 mm and 25.6 mm showing the need for electrode length to be as short as 20 mm for the smallest and 25 mm for the largest IP type II cochleae. In the case of IP type I, a 16 mm-long electrode might be necessary for the smallest cochlea and a 25 mm-long electrode for the largest cochlea. For cavity-type malformations, a short electrode length of 13 mm seems to match the circumference of the smallest cavity, and a longer electrode length of 33 mm would be required to match the largest cavity. For IP type III, a short electrode length of 19 mm may match the smallest cochlea and a 24 mm-long electrode may match the largest cochlea. A complete list of electrode lengths from all four CI manufacturers is provided in a recent report by Dhanasingh et al[8]. As most IEM types lack central modiolus trunk, placing the electrode along the OW seem to be logical. We believe that our research finding of estimating OWL for a safe electrode insertion

depth along with the developed software application will add practical relevance to the CI field, especially in the niche topic of IEM.

One of the key limitations of this study is that we deliberately excluded the cochlear hypoplasia malformation type because of high variation in the overall morphology of the inner ear, which limited us from formulating a mathematical equation to estimate the OWL for this malformation type. Another limitation is the lack of clinical validation of the proposed mathematical equations as this was a retrospective study with the absence of post-operative images in most of the cases. Our future work will focus on validating the clinical accuracy of the mathematical equations to choose the electrode length based on the estimated OWL.

Conclusion

To the best of our knowledge, this is the first study to provide a practical solution for estimating the OWL in IEM types to ensure safe electrode insertion depth. We found a consistent extension of the OWL for an angular depth of 540° in the EVAS type, 360° in IP type I, 450° in IP type II, and approximately 540° in IP type III. Determining the circumference of the cavity is important for choosing an appropriate electrode length in cavity-type malformation. The software application used to estimate the OWL could be useful for choosing the electrode length to cover the effective insertion depth in different IEMs.

Data availability

The datasets used and analyzed during the current study are available from the corresponding author on reasonable request.

Received: 24 June 2024; Accepted: 28 October 2024
Published online: 09 November 2024

References

1. Entwisle, L. K., Warren, S. E. & Messersmith, J. J. Cochlear implantation for children and adults with severe-to-profound hearing loss. *Semin Hear.* **39**, 390–404 (2018).
2. Virzob, C.R.B., Poenaru, M., Morar, R., Horhat, I.D., Balica, N.C., Prathipati, R., Moleriu, R.D., Toma, A.O., Juganaru, I., Bloanca, V., Chicin, G.N., Fericean, R.M., Domuta, E.M., Iurciuc, M., Iurciuc, S. Efficacy of Bilateral Cochlear Implantation in Pediatric and Adult Patients with Profound Sensorineural Hearing Loss: A Retrospective Analysis in a Developing European Country. *J. Clin. Med.* **12** (8), 2948. https://doi.org/10.3390/jcm12082948 (2023). PMID: 37109284; PMCID: PMC10144087.
3. World Health Organization. WHO: 1 in 4 people projected to have hearing problems by 2050. (2021). https://www.who.int/news/item/02-03-2021-who-1-in-4-people-projected-to-have-hearing-problems-by-2050
4. Zhao, E. E. et al. Association of patient-related factors with adult cochlear implant speech recognition outcomes: a meta-analysis. *JAMA Otolaryngol. Head Neck Surg.* **146**, 613–620 (2020).
5. Bernhard, N. et al. Duration of deafness impacts auditory performance after cochlear implantation: a meta-analysis. *Laryngoscope Investig Otolaryngol.* **6**, 291–301 (2021).
6. Kurz, A., Grubenbecher, M., Rak, K., Hagen, R. & Kühn, H. The impact of etiology and duration of deafness on speech perception outcomes in SSD patients. *Eur. Arch. Otorhinolaryngol.* **276**, 3317–3325 (2019).
7. Gaurav, V., Sharma, S. & Singh, S. Effects of age at cochlear implantation on auditory outcomes in cochlear implant recipient children. *Indian J. Otolaryngol. Head Neck Surg.* **72**, 79–85 (2020).
8. Dhanasingh, A. et al. Cochlear implant electrode design for safe and effective treatment. *Front. Neurol.* **15**, 1348439 (2024).
9. Breitsprecher, T. M. et al. Effect of Cochlear Implant Electrode insertion depth on Speech Perception outcomes: a systematic review. *Otol Neurotol Open.* **3** (4), e045 (2023).
10. Escudé, B. et al. The size of the cochlea and predictions of insertion depth angles for cochlear implant electrodes. *Audiol. Neurootol.* **11** (Suppl 1), 27–33 (2006).
11. Alexiades, G., Dhanasingh, A. & Jolly, C. Method to estimate the complete and two-turn cochlear duct length. *Otol. Neurotol.* **36**(5), 904-7. https://doi.org/10.1097/MAO.0000000000000620 (2015).
12. Singh, A. et al. Radiographic measurement of cochlear duct length in an indian cadaveric population - importance of custom fit cochlear implant electrodes. *Int. Arch. Otorhinolaryngol.* **24** (4), e492–e495 (2020).
13. Alshalan, A. et al. Method to estimate the basal turn length in inner ear malformation types. *Sci. Rep.* **13**, 66 (2023).
14. Sennaroğlu, L. & Bajin, M. D. Classification and current management of inner ear malformations. *Balkan Med. J.* **34**, 397–411 (2017).
15. Warnecke, A., Giesemann, A. Embryology, Malformations, and Rare Diseases of the Cochlea. *Laryngorhinootologie* **100**(S 01), S1-S43. https://doi.org/10.1055/a-1349-3824. (2021).
16. Dhanasingh, A. Embryology of inner ear malformation types and its radiological relevance in Cochlear Implantation for Common Cavity Deformity (ed Li, Y.) (Springer, (2022).
17. Weiss, N. M., Langner, S., Mlynski, R., Roland, P. & Dhanasingh, A. Evaluating common cavity cochlear deformities using CT images and 3D reconstruction. *Laryngoscope.* **131**, 386–391 (2021).
18. Dhanasingh, A. E. et al. A novel three-step process for the identification of inner ear malformation types. *Laryngoscope Investig Otolaryngol.* **7**, 2020–2028 (2022).
19. Dhanasingh, A., Dietz, A., Jolly, C. & Roland, P. Human inner-ear malformation types captured in 3D. *J. Int. Adv. Otol.* **15**, 77–82 (2019).
20. Alsughayer, L., Al-Shawi, Y., Yousef, M. & Hagr, A. Cochlear electrode array tip fold-over in incomplete partition-I - a case report. *Int. J. Pediatr. Otorhinolaryngol.* **139**, 110438 (2020).
21. Adunka, O., Unkelbach, M. H., Mack, M. G., Radeloff, A. & Gstoettner, W. Predicting basal cochlear length for electric-acoustic stimulation. *Arch. Otolaryngol. Head Neck Surg.* **131**, 488–492 (2005).
22. Dhanasingh, A. E., Rajan, G. & van de Heyning, P. Presence of the spiral ganglion cell bodies beyond the basal turn of the human cochlea. *Cochlear Implants Int.* **21**, 145–152 (2020).
23. Li, H. et al. Three-dimensional tonotopic mapping of the human cochlea based on synchrotron radiation phase-contrast imaging. *Sci. Rep.* **11** (1), 4437. https://doi.org/10.1038/s41598-021-83225-w (2021). PMID: 33627724; PMCID: PMC7904830.
24. Graham, J. M., Phelps, P. D. & Michaels, L. Congenital malformations of the ear and cochlear implantation in children: review and temporal bone report of common cavity. *J. Laryngol Otol Suppl.* **25**, 1–14 (2000).
25. Yamazaki, H. et al. Electrically evoked auditory brainstem response-based evaluation of the spatial distribution of auditory neuronal tissue in common cavity deformities. *Otol Neurotol.* **35**, 1394–1402 (2014).

26. Monsanto, R. D. C. et al. Histopathology of inner ear malformations: potential pitfalls for cochlear implantation. *Otol Neurotol.* **40**, e839–e846 (2019).

Author contributions

Afrah A: Data collection, image analyses, writing, literature summary. Yassin A and Asma A: Statistical analyses, study design, writing, critical review. Francesco S and Anandhan D : Data collection, image analyses, statistical analyses, literature summary, writing, critical review. Salman A and Fida A : study design, writing . Farid A and Abdulrahman A : writing, critical review.

Declarations

Competing interests

Yassin Abdelsamad and Anandhan Dhanasingh work for MED-EL GmbH purely in a research role with no sales and marketing duties, the remaining authors have no conflicts of interest to declare.

Additional information

Correspondence and requests for materials should be addressed to A.A.

Reprints and permissions information is available at www.nature.com/reprints.

Publisher's note Springer Nature remains neutral with regard to jurisdictional claims in published maps and institutional affiliations.